This is a repository copy of *From Au-Thiolate Chains to Thioether Sierpiński Triangles: The Versatile Surface Chemistry of 1,3,5-Tris(4-Mercaptophenyl)Benzene on Au(111)*.

Article:

From Au-Thiolate Chains to Thioether Sierpiński Triangles: The Versatile Surface Chemistry of 1,3,5-Tris(4-Mercaptophenyl)Benzene on Au(111)

Atena Rastgoo-Lahrood,[†] Natalia Martsinovich,[‡] Matthias Lischka,[†] Johanna Eichhorn,[†] Pawel Szabelski,[#] Damian Nieckarz,[˩] Thomas Strunskus,[⊥] Kalpataru Das,[§] Michael Schmittel,[§] Wolfgang M. Heckl[†], and Markus Lackinger[†*]

[†]Department of Physics, Technische Universität München, James-Franck-Str. 1, 85748 Garching, Germany; Nanosystems Initiative Munich and Center for NanoScience (CeNS), Schellingstr. 4, 80799 Munich, Germany;

Deutsches Museum, Museumsinsel 1, 80538 Munich, Germany;

[‡]Department of Chemistry, University of Sheffield, Sheffield S3 7HF, UK;

[#]Department of Theoretical Chemistry, Maria Curie-Skłodowska University, Pl. M.C. Skłodowskiej 3, 20-031 Lublin, Poland;

[˩]Supramolecular Chemistry Laboratory, University of Warsaw, Biological and Chemical Research Centre, Zwirki i Wigury 101, 02-089 Warsaw, Poland;

[⊥]Institute for Materials Science − Multicomponent Materials, Christian-Albrechts-Universität zu Kiel, Kaiserstr. 2, 24143 Kiel, Germany;

§Center of Micro- and Nanochemistry and Engineering, Organische Chemie I,

Universität Siegen, Adolf-Reichwein-Str. 2, 57068 Siegen, Germany,

ABSTRACT

Self-assembly of 1,3,5-*tris*(4-mercaptophenyl)benzene (TMB) – a three-fold symmetric, thiol functionalized aromatic molecule – was studied on Au(111) with the aim to realize extended Au-thiolate linked molecular architectures. The focus lay on resolving thermally activated structural and chemical changes by a combination of microscopy and spectroscopy. Thereby Scanning Tunneling Microscopy provided submolecularly resolved structural information, while the chemical state of sulfur was assessed by X-ray Photoelectron Spectroscopy. Directly after room temperature deposition only less well ordered structures were observed. Mild annealing promoted the first structural transition into ordered molecular chains, partly organized in homochiral molecular braids. Further annealing led to self-similar Sierpiński triangles, while annealing at even higher temperatures again resulted in mostly disordered structures. Both the irregular aggregates observed at room temperature and the chains were identified as metal-organic assemblies, whereby two out of the three intermolecular binding motifs are energetically equivalent according to Density Functional Theory simulations. The emergence of Sierpiński triangles is driven by a chemical transformation, *i.e.* the conversion of coordinative Au-thiolate to covalent thioether linkages, and can be further understood by Monte Carlo simulations. The great structural variance of TMB on Au(111) can on one hand be explained by the energetic equivalence of two binding motifs. On the other hand, the unexpected chemical transition even enhances the structural variance and results in thiol-derived covalent molecular architectures.

The notorious affinity of thiols to gold is beneficial for molecular nano-science.[1] Important examples include ligation of gold nanoparticles,[2, 3] two probe conductance measurements of single molecules,[4-7] and surface functionalization of Au(111) by Self-Assembled Monolayers (SAMs).[8, 9] All of these applications rely on anchoring *via* strong Au-thiolate bonds. Even though thiolate SAMs are widespread, structural details of the anchor bond were discussed controversially for a long time. Yet, a consensus seems to be reached insofar as Au-thiolate complexes formed with gold adatoms play an important role.[10] The promising properties of RS-Au-SR linkages, in particular their electric conductance and their ability to form spontaneously on Au(111) motivated the present study with the aim to utilize these linkages for extended molecular nanostructures. To this end 1,3,5-*tris*(4-mercaptophenyl)benzene (TMB) as a threefold functionalized and suitable model compound for network formation is studied on Au(111). Owing to both the extended triphenylbenzene backbone and the three-point anchoring *via* thiolate-surface bonds, planar adsorption is anticipated as an important prerequisite for extended networks. In contrast to SAMs, where the prevalent monothiols adopt upright adsorption geometries, the linkages here are directly accessible by high resolution Scanning Tunneling Microscopy (STM). Our previous study of TMB on Cu(111) showed an interesting temperature evolution: After room temperature deposition deprotonated TMB anchored *via* covalent copper-thiolate bonds to the surface, thereby forming a densely packed regular structure dominated by molecule-surface interactions.[11] Mild annealing converted this initial structure into two coexisting polymorphs stabilized by lateral coordination bonds. In the light of these results, the

present study also aims at comparing self-assembly and thermally activated surface chemistry of TMB on more inert Au(111) surfaces, that, however, feature a high Au-thiolate bond strength.

RESULTS AND DISCUSSION

Room temperature deposition of TMB onto Au(111) resulted in scattered aggregates as shown by the STM images in Figure 1. High resolution reveals a seemingly irregular arrangement of interconnected molecules. Yet, these structures feature only three basic intermolecular binding motifs (*cf.* Figure 1b) that can be further classified into singly and doubly joined TMB units. The term „motif" is used in a broader sense here, also including different configurations of chemically equivalent intermolecular bonds. Twofold connected molecules are linked *via* two of their mercaptophenyl groups, thereby enclosing a small pore. This motif 1 is mirror symmetric and features a center-to-center distance of (1.19 ± 0.05) nm (DFT: 1.19 nm). Singly connected molecules are linked *via* only one of their mercaptophenyl groups, whereby two different types can be distinguished: motif 2 interconnects appear nearly straight (closer inspection reveals a kink), whereas motif 3 exhibits a hairpin bend. The experimental direct center-to-center distance of molecules in motif 2 amounts to (1.79 ± 0.09) nm (DFT: 1.74 nm) with a lateral offset of $(0.41 \text{ nm} \pm 0.08)$ nm (DFT: 0.46 nm). Binding motif 2 lacks mirror symmetry, but exhibits twofold rotational symmetry, and is accordingly prochiral on the surface. Motif 3 is again in most cases mirror symmetric with a center-to-center distance of (1.21 ± 0.03) nm (DFT: 1.16 nm) and a bending angle of $64.5° \pm 6°$. Distances in parentheses refer to density functional theory (DFT) simulations based on S-Au-S linkages (*vide infra*). Statistical analysis of more than 800 linkages resulted in 41.0% motif 1, 43.2% motif 2, and 15.8% motif 3. Yet the scattering between different data sets is relatively large. For instance, the probability for finding motif 1

varied from ~36% to ~46% between different data sets, however, the lower probability of motif 3 is a common finding. Albeit all intermolecular connections correspond to one of these three motifs, not all thiolate groups form intermolecular bonds. Examples for such "loose ends" are marked in Figure 1b. Yet, the exact chemical nature of these termini is not clear. Most likely, these thiol groups are similarly deprotonated and bind to Au surface or adatoms.
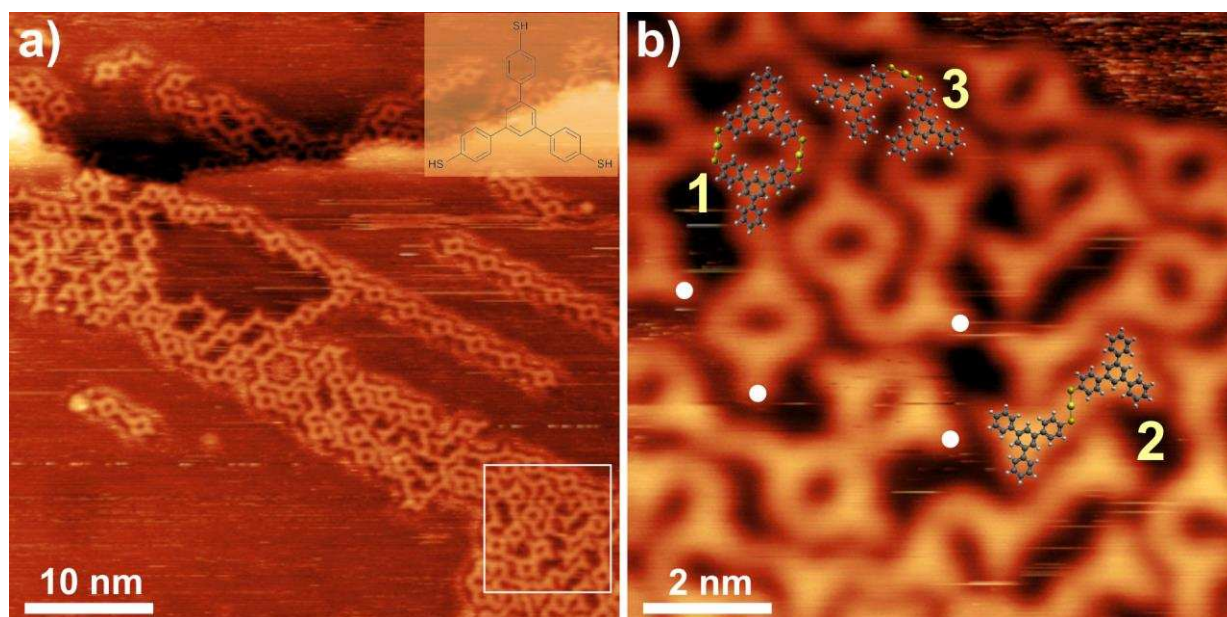
Figure 1. STM images acquired after room temperature deposition of TMB onto Au(111) (a) Overview (V_T = +1.83 V, I_T = 48.7 pA). Upper right insert: chemical structure of TMB. (b) Close-up of the area marked in (a) (V_T = +1.66 V, I_T = 48.3 pA). This less regular arrangement features binding motifs 1 - 3, respective examples are overlaid by DFT-optimized dimers based on S-Au-S linkages. The white dots highlight "loose ends", where thiolate groups do not form further intermolecular bonds.

Emergence of non-crystalline structures is an interesting, occasionally observed phenomenon in self-assembly, indicating either metastability or energetic equivalency of different binding motifs.[12] To overcome a conceivable kinetic trapping, samples were stepwise annealed at 200 °C,

250 °C, and 300 °C for ~30 min, and STM data were acquired after each annealing step. Heating at 200 °C resulted in mostly ordered 1D structures (*cf.* Figure 2), *i.e.* molecular chains or grouped chains (molecular braids). Shorter chains are already recognizable after room temperature deposition in Figure 1a, yet heating leads to more extended and more regular structures. Longer chains align along the Au(111) herringbone reconstruction, whereas shorter chain segments or chains in the vicinity of step-edges locally modify the herringbone reconstruction (*cf.* Supporting Information) as similarly observed for alkanethiols on Au(111).[10] Two different types of chains can be distinguished: Type A chains (Figure 2b) appear mostly as molecular braids, whereas type B chains (Figure 2c) were only observed as individuals.
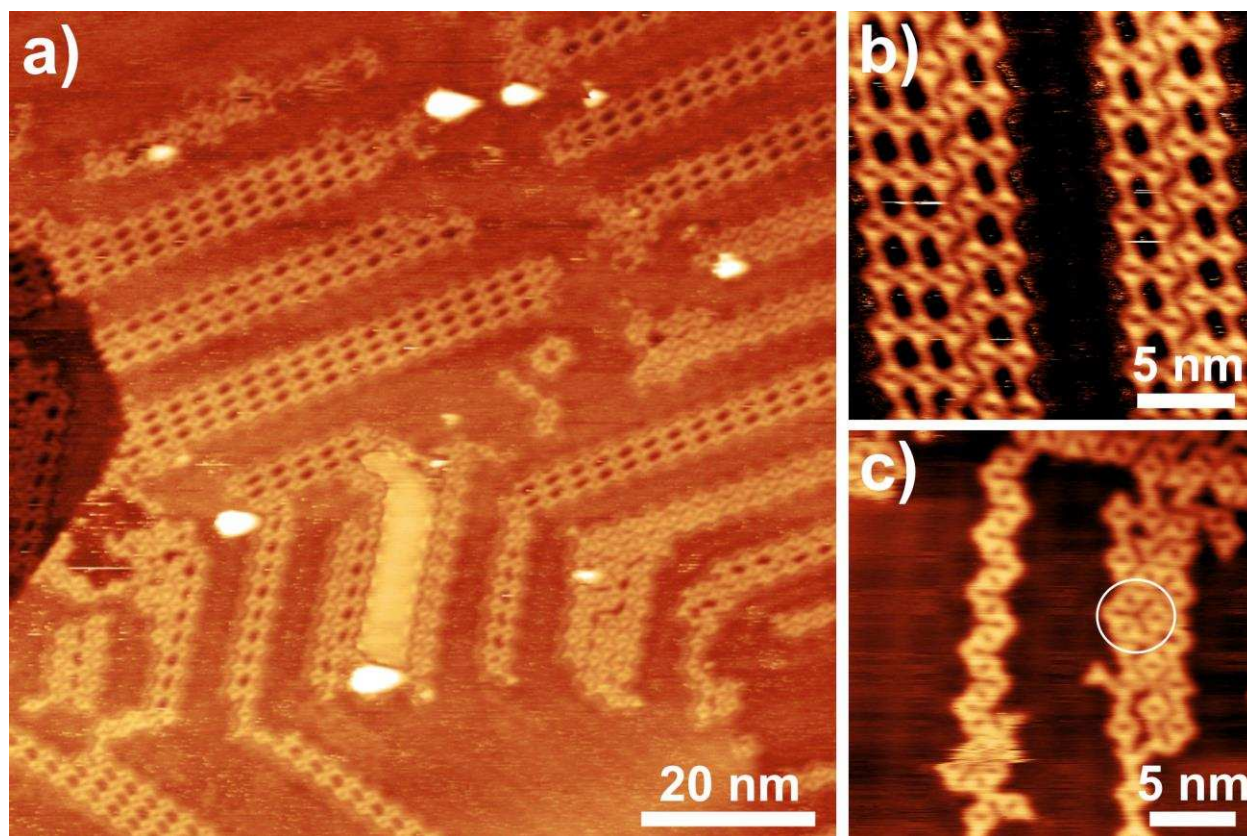

Figure 2. STM images of TMB on Au(111), acquired after annealing at 200 °C. (a) Overview (V_T = +1.64 V, I_T = 38.1 pA). (b) Close-up of braided type A chains (V_T = +1.64 V, I_T = 38.5

pA). (c) Close-up of a single type B chain (left hand side), alongside with frequently observed less regular aggregates (right hand side) (V_T = +1.79 V, I_T = 37.1 pA). The white circle marks a hexameric closed-ring structure.

Both types of chains feature alternating orientations of molecules. In type A chains binding motifs 1 and 2 alternate, whereby homochirality is observed along all motifs 2. Interestingly, the homochirality of a single type A chain is preserved even at the next higher level of organization, *i.e.* the molecular braids. A noteworthy further observation is the defined phase relation between adjacent chains in the braids, either aligned or shifted by half a repeat distance, examples for both cases are depicted in Figure 2b. Type B chains are comprised of an alternating sequence of binding motifs 1 & 3, but are less regular with only short periodic segments. The right hand side of Figure 2c also shows less well ordered structures that predominantly consist of alternating binding motifs 1 and 3, yet with interspersed motif 2 defects. Since motif 3 can bend in either direction, also curled up or even closed-ring structures were observed, an example is marked in Figure 2c. Remarkably, the structural versatility obtained after annealing at 200 °C results from just alternating motif 1 with either motif 2 or 3.

An unexpected structural transition occurred after sample annealing at 250 °C, converting the chains into mostly triangular aggregates of various sizes. An overview STM image is shown in Figure 3 (*cf.* Supporting Information for further images). The depicted triangles feature just one intermolecular binding motif 4 (*cf.* Figure 3b), where connected molecules have similar orientation and a center-to-center distance of (1.31 ± 0.06) nm. Hence, the transition from chains to triangles is also a transition from the co-existence of three binding motifs to exclusively one binding motif. The smallest triangular unit consists of three molecules. However, these trimeric

triangles organize into larger self-similar triangles – a molecular realization of so called Sierpiński triangles (ST).
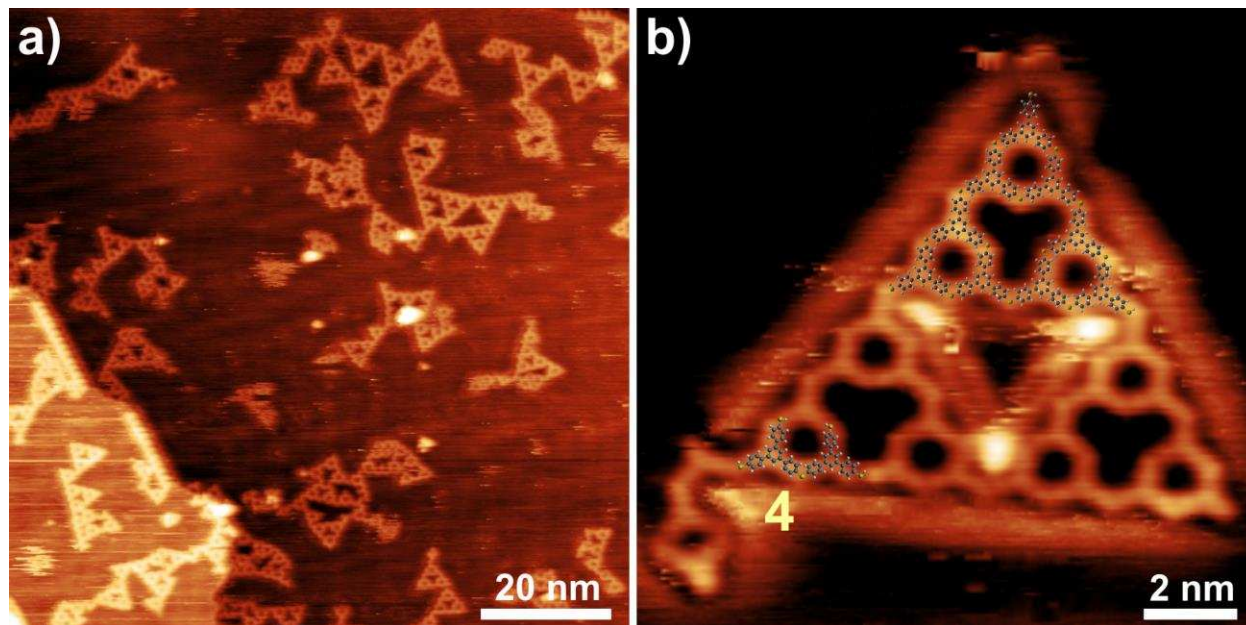
Figure 3. STM images of TMB on Au(111), acquired after annealing at 250 °C. (a) Overview (V_T = +1.80 V, I_T = 39.4 pA). (b) Close-up of a second generation ST (V_T = -1.63 V, I_T = 38.1 pA). The upper part was overlaid to scale with a DFT-optimized structure of a covalent first generation ST. The lower left corner of the triangle is overlaid with a DFT-optimized motif 4 dimer featuring a C-S-C interlink.

Molecular materializations of regular fractals have recently experienced increasing interest, not at least because they are particularly suitable for high resolution microscopy. Sierpiński hexagons could be synthesized in solution from bis-terpyridine building blocks coordinatively bound to 36 Ru and 6 Fe centers and imaged by STM after subsequent deposition onto Au(111).[13] More recently, self-assembly of STs directly on surfaces has emerged as alternative approach. Feasibility was first demonstrated with dibromo-terphenyl and dibromo-quaterphenyl

on Ag(111), resulting in STs based on hydrogen and halogen-bonds.[14] However, other types of non-covalent intermolecular bonds also proved suitable. For instance, using 4,4"-dihydroxy-1,1':3',1"-terphenyl on Au(111), Zhang *et al.* demonstrated hydrogen bonded STs.[15] Interestingly, co-deposition of Fe atoms similarly resulted in STs on Ag(111) and Ag(100), yet with enhanced stability through the formation of Fe-O coordination bonds.[16] Moreover, metal-organic STs could also be prepared by co-adsorption of 4,4"-dicyano-1,1':3',1"-terphenyl and Fe or Ni onto Au(111).[17,18] All these examples utilize V-shaped ditopic linkers with *m*-terphenyl backbone, whereby the key to ST formation is the expression of threefold nodes either by cyclic halogen, hydrogen, or metal-coordination bonds. On the contrary, Gu *et al.* proposed synthesis of covalent STs by using Schiff-base coupling of 1,3,5-*tris*(4-aminophenyl)benzene (TAPB) and 4,4"-dialdehyde-1,1':3',1"-terphenyl (TPDAL) on Au(111).[19] Here the required threefold symmetry originates from TAPB, whereas the imine linkages to three again V-shaped ditopic TPDAL linkers result in a similar topology as for the examples above. This innovative approach yielded covalent STs, however, the formation of larger STs requires a specific conformation of the secondary TAPB(TPDAL)$_3$ building unit, and the frequent occurrence of deviating aggregates as *e.g.* homotactic nodes can disrupt the ST growth. In this respect, the use of TMB as a single threefold symmetric tecton appears advantageous for ST formation. For TMB on Au(111) we observe STs up to the second generation consisting of 27 molecules. In retrospect, the possibility of forming STs from TMB was already alluded in our earlier work on Ag(111), where cyclic trimers, but no larger STs were observed after annealing.[11] However, the concomitant formation of various other less well defined molecular aggregates presumably prevented the formation of larger STs.

Besides triangles, structurally deviant type C chains were also observed (Figure 4). In contrast to type A and B chains, these chains were only found along step-edges, suggesting an important role as template or for stabilization. Type C chains are solely comprised of binding motif 4, yet arranged in a periodic linear fashion. Aggregation into pairs similarly occurred for type C chains, but only on the upper and lower side of step-edges. The opposite orientation and phase shift of half a repeat distance resembles a molecular zipper.
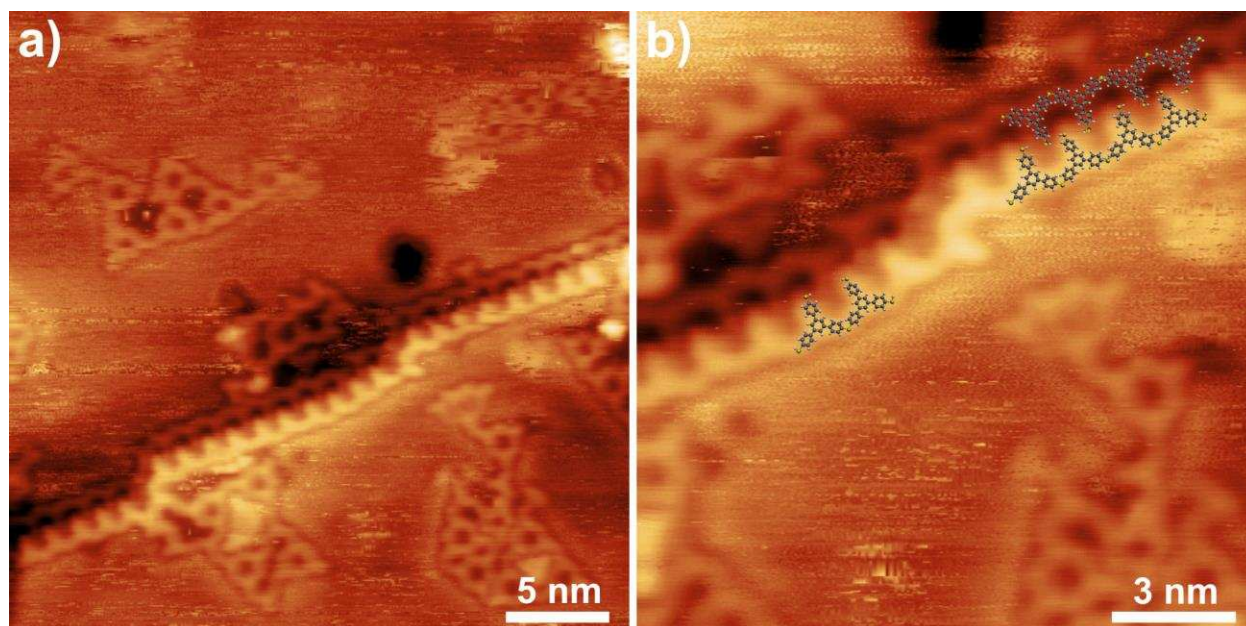
Figure 4. STM images of pairs of type C chains ("molecular zipper") formed on Au(111) step-edges after annealing at 250 °C. (a) Overview (V_T = +1.00 V, I_T = 40.0 pA). (b) Close-up of the molecular zipper overlaid with motif 4 dimers (V_T = +1.00 V, I_T = 40.0 pA).

Sample annealing at even higher temperatures of 300 °C diminished the triangles, and also resulted in less well ordered structures as illustrated in the STM images in Figure 5. Close-up images in Figure 5b and 5c show details: Dimers of oppositely oriented molecules as in motif 2, yet with a reduced center-to-center distance of (1.32 ± 0.06) nm and a straight geometry were

regularly observed in independent experimental runs (*cf.* Supporting Information). Moreover, also remnants of triangles, chains, and other motif 4 sequences were found across terraces.
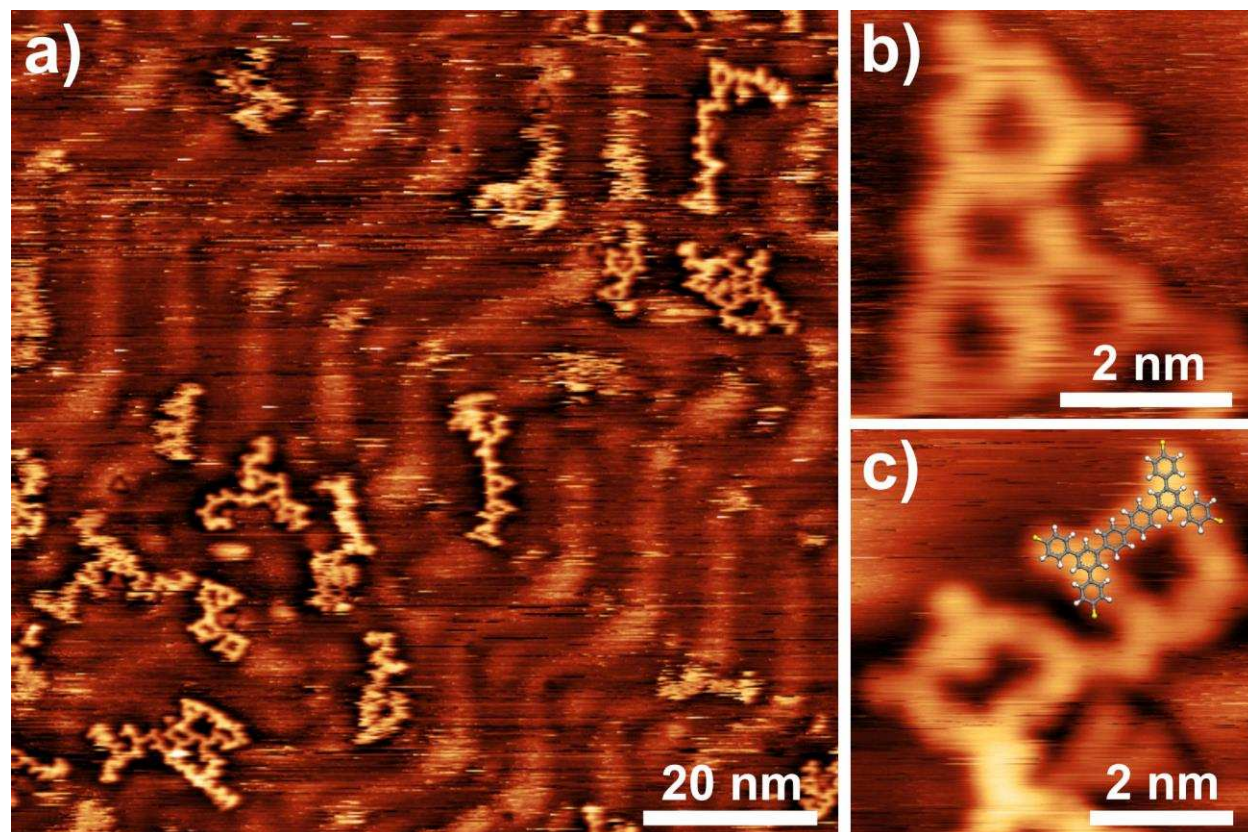
Figure 5. STM images acquired after annealing at 300 °C. (a) Overview (V_T = +1.63 V, I_T = 50.8 pA). (b) Close-up of a triangle remnant (V_T = +1.62 V, I_T = 39.1 pA). (c) Close-up of a straight molecular dimer (V_T = +1.69 V, I_T = 40.2 pA) overlaid with a C-C linked dimer.

The first important step to understand self-assembly of TMB on Au(111) is to resolve these structures, *i.e.* to clarify the nature of the intermolecular bonds. The most likely candidates are S-Au-S linkages or disulfide bridges. A clear contrast feature of Au atoms involved in coordination was not observed for motifs 1 – 4, hence a distinction based solely on STM contrast is not easily possible. Albeit S-Au-S linkages and disulfide bridges can be distinguished by their markedly

different bond lengths,[11] complementary data on the chemical state of sulfur is potentially useful. To this end, XPS measurements were carried out after room temperature deposition and after each successive annealing step (Figure 6). The XP spectrum of S 2p after room temperature deposition features a spin-orbit doublet that can be fitted with a single chemical sulfur species. This results in a S $2p_{3/2}$ binding energy of 162.1 eV, in good agreement with reported values of 162.0 eV for Au-sulfur bonds in thiophene and alkanethiol SAMs[20, 21] as well as 162.3 eV for benzenethiol on Au(111).[22] However, XPS does not allow distinguishing whether the thiolates coordinate to gold surface atoms or adatoms. On Cu(111), TMB room temperature deposition resulted in bonds with surface atoms.[11] According to a full structural refinement by quantitative LEED and in agreement with comprehensive DFT simulations, the Cu-thiolate bonds were localized slightly off center a fcc threefold hollow site.[23] Here the missing structural information on the gold-thiolate bond can be deduced from STM: on Au(111) molecules appear interconnected without any apparent gaps or dips between them, whereas on Cu(111) single molecules were clearly resolved as separate entities. Combination of XPS (indicating Au-thiolate linkages) and STM (indicating direct intermolecular bonds) allows us to conclude that the room temperature structures are stabilized by coordinative S-Au-S linkages as similarly proposed for low coverages of benzenethiol on Au(111).[24] Since motifs 1 - 3 coexist with notable proportions, this conclusion equally applies to all motifs.
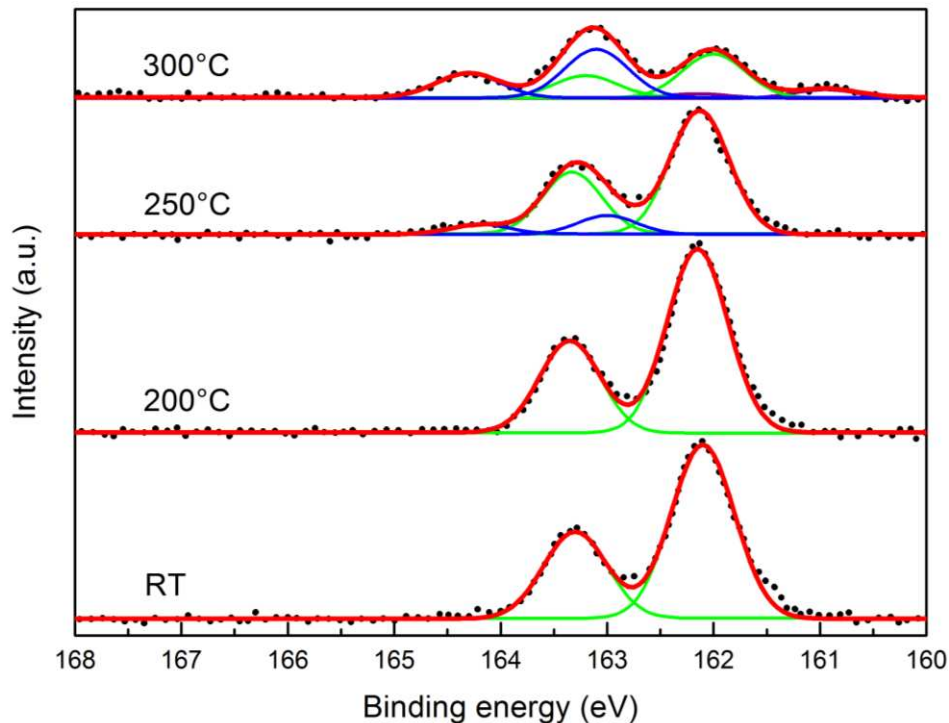
Figure 6. XP spectra of S 2p acquired after room temperature deposition and after annealing at 200 °C, 250 °C, and 300 °C. All annealing steps were carried out successively with the same sample, and spectra were acquired after cooling down to at least room temperature or below. S 2p consists of a 1/2 and 3/2 spin-orbit doublet. Spectra were fitted with a fixed energy separation of 1.2 eV and a fixed peak area ratio for $p_{1/2}$: $p_{3/2}$ of 1 : 2. After annealing at 250 °C a second doublet appears at higher binding energies. After annealing to 300 °C this doublet increases in intensity and a third doublet appears at lower binding energy.

XP spectra acquired after room temperature deposition and after sample annealing to 200 °C are virtually identical, suggesting an unaltered chemical environment of sulfur. Consequently, also type A and B chains are stabilized by S-Au-S linkages. This assignment is consistent with STM, as both types of molecular chains are based on the same binding motifs already present at room temperature. To infer further structural details, DFT simulations of the three basic motifs and their periodic sequences based on S-Au-S linkages were performed in the gas phase; the

13

optimized structures are depicted in Figure 7. All three dimer motifs are non-planar in the gas

phase, but the energy costs of planarization are comparatively small (0.29 eV for motif 1 and

0.40 .. 0.43 eV for motifs 2 and 3). Moreover, inclusion of the less planar motif 3 dimer into

periodic chains leads to a more planar structure even in the gas phase. Scaled overlays of these S-

Au-S linked basic motifs result in perfect matches, as already demonstrated in Figure 1. The S-

Au bond lengths correspond to 0.241 nm in all planarized motifs. In order to estimate the surface

influence, additional simulations of adsorbed motif 2 dimers on Au(111) were carried out, and

resulted in a slightly reduced S-Au bond length of 0.233 nm (*cf.* Supporting Information).

Therefore it was assumed that all peripheral thiolate groups also bind to Au adatoms. This

additional constraint resulted in a non-planar adsorption geometry with tilted phenyl rings, and

consequently in a relatively large average carbon adsorption height of 0.351 nm with a large

standard deviation of 0.051 nm. In contrast, similar simulations of a hydrogen passivated motif 2

dimer that is not covalently anchored resulted in a mostly planar structure with virtually similar

S-Au bond length (0.234 nm), but a reduced average carbon adsorption height of 0.319 nm and

lower standard deviation of 0.015 nm.

Similarly, periodic type A and B chains were simulated in the gas phase. The optimized

theoretical repeat distances of (2.87 ± 0.03) nm and (3.60 ± 0.02) nm agree well with

experimental values of (2.84 ± 0.08) nm and (3.53 ± 0.07) nm, respectively. This concurrence

provides strong evidence for the proposed chain structures as alternating sequences of motif 1

with either motif 2 or 3. However, total energies of the chains in DFT vary only weakly with

repeat distance ($\Delta E \leq$ 0.1 eV for ±0.2 Å), resulting in larger uncertainties. In any case, covalent

disulfide bridges can be excluded due to their significantly shorter bond length, and because they

would appear in XPS as new sulfur species at higher binding energies.[25] Notably, with reference

to protonated TMB and H_2 as deprotonation product, motif 2 and 3 both feature a similar binding energy of (1.71 ± 0.1) eV, whereas motif 1 is more stable with a binding energy of 2.77 eV. The intermediate bond strength of the S-Au-S linkages facilitates dynamic rearrangements at room temperature (*cf.* Supporting Information). Moreover, both motif 2 and motif 3 feature an almost linear S-Au-S arrangement and can be viewed as *syn* and *anti* conformers, as previously proposed for phenyl-S-Au-S-phenyl complexes on Au(111).[24]

These DFT results can already explain the observed chain formation: Owing to its higher stability, motif 1 is preferentially formed, but as it requires two mercaptophenyl groups per molecule it is not suitable for the formation of extended structures. However, motif 1 dimers can further interlink *via* their free mercaptophenyl groups. Thereby, the energetic equivalency of motifs 2 & 3 gives rise to the coexistence of both motifs, and hence the coexistence of type A and B chains. An interesting difference to previous results on Cu(111) is that on Au(111) only one Au adatom is involved per coordinative bond, whereas on Cu(111) straight intermolecular bonds with two Cu adatoms were proposed.
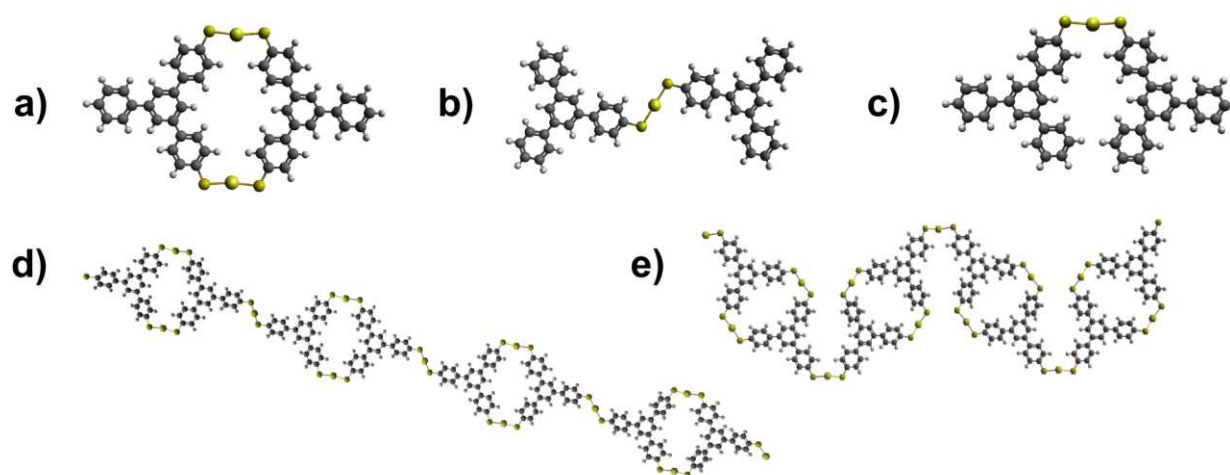
Figure 7. DFT-optimized structures in the gas phase of (a) – (c) planarized motifs 1 – 3 based on S-Au-S linkages and (d) / (e) periodic type A and B chains comprised of an alternating sequence of motif 1 and either motif 2 or 3.

First changes in XPS were observed after annealing to 250 °C. A second chemically shifted species appears at a higher S 2 $p_{3/2}$ binding energy of 163.0 eV and a peak area fraction of 13.3%. According to the previous assignment, the majority of sulfur is still in Au-thiolate bonds, suggesting that also the STs may be stabilized by S-Au-S linkages. Additional annealing at 300 °C results in further changes. The sulfur species at higher binding energy increases in intensity, and an additional species with lower S 2 $p_{3/2}$ binding energy of 161.0 eV appears. In the literature this species is assigned to chemisorbed sulfur on Au(111) with a reported binding energy of 160.95 eV.[22, 26, 27] According to a quantitative analysis 43 % of sulfur is still in S-Au-S linkages, 48 % correspond to the unassigned species, the remaining 9 % correspond to chemisorbed sulfur.

Since there is no drastic change in XPS upon annealing at 250 °C – the temperature where the ST emerged – the initial assumption was that motif 4 is chemically equivalent to motif 2 and 3, *i.e.* molecules are connected *via* S-Au-S linkages. However, this hypothesis is untenable for two reasons: Motif 4 requires a S-Au-S angle of 120°. Yet, according to DFT S-Au-S strongly prefers a nearly linear configuration as in motifs 1 - 3, resulting in instability of the 120° angle. Nevertheless, a cyclic triangular structure of three molecules, *i.e.* a zero generation ST, with nearly linear S-Au-S linkages could be stabilized in simulations, however at the expense of a highly non-planar geometry. Hence, formation of such structural units appears highly unlikely. The second argument against Au-thiolate bonds in the ST is a significant size discrepancy to the experiment. A scaled overlay of a simulated metal-organic first generation ST with STM data results in a notable size mismatch, and thereby excludes this type of interlink (*cf.* Supporting

Information). Yet, a perfect size match is obtained with a new type of covalent thioether C-S-C interlink, as demonstrated by the scaled overlay in Figure 3b with a DFT-optimized structure of a corresponding first generation ST. Not only the bond lengths match very well, but also the bulge from the non-linear C-S-C configuration is consistently present in both simulation and experiment. In addition, the formation energy of this first generation ST in the gas phase from nine molecules was estimated by DFT. Therefore, fully protonated TMB molecules were taken as reference state and H_2S molecules as formal reaction byproduct, because the formation of each C-S-C thioether linkage releases two hydrogen and one sulfur atom. This results in a total stabilization energy of -0.45 eV for the entire ST, corresponding to -0.038 eV for each of the twelve thioether bonds, respectively. The proposed thioether C-S-C interlink can formally be derived from the original thiolate C-S-Au-S-C linkages by ejecting Au-S. Even though the geometric comparison unequivocally confirms the thioether bonds, important questions arise: (1) How does this chemical change affect XPS? (2) By what chemical process are the coordinative S-Au-S linkages converted into covalent C-S-C bonds? (3) How does this bond conversion lead to the observed fractals?

Chemical core level shifts in XPS originate from changes of the valence electron configuration. Consequently, even a change of bond type might not necessarily result in a detectable shift, provided that the valence electron configuration does not change significantly. For thioethers adsorbed on Au(111) the reported S $2p_{3/2}$ binding energies of 162.0 eV are virtually identical to those of Au-thiolates.[28] Consequently, the proposed chemical conversion from Au-thiolate to thioether linkages cannot directly be monitored by XPS on a gold surface. The absence of a pronounced sulfur core level shift is partly related to the comparable electron affinities of carbon and gold, 2.55 *versus* 2.4 on the Pauling scale. The chemical environment of sulfur changes from

C-S-Au in the Au-thiolate to C-S-C in the thioether, *i.e.* sulfur exchanges Au for C as bond partner. This implies minor changes of the valence electron configuration, hence small core level shifts in XPS. The second reason is that the thiolates as well as the thioethers are both chemisorbed, *i.e.* sulfur also features a hardly affected bond to the gold surface in both cases. The proposed conversion, however, also results in ejected sulfur. Accordingly, a conceivable core level shift of this species allows monitoring the reaction progress in XPS by tracing the byproduct.

The following hypothesis also closely relates to the driving force of this chemical transition. The conversion of coordinative to covalent bonds occurs at higher surface temperatures with enhanced Au adatom density. Hence, interactions of the coordinatively unsaturated Au adatoms with the sulfur atoms of the C-S-Au-S-C linkage become more likely and such binding should weaken the C-S bond. Finally, Au-S-Au is ejected along with C-S bond cleavage and the two remaining fragments combine to afford the thioether linkage. The overall conversion can be summarized as:

$$C\text{-}S\text{-}Au\text{-}S\text{-}C + Au \rightarrow C\text{-}S\text{-}C + Au\text{-}S\text{-}Au$$
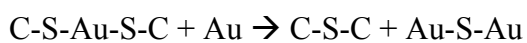
DFT simulations suggest that this chemical conversion is enthalpically almost neutral with an overall energy change of -0.02 eV in the gas phase. However, entropy is gained from releasing Au-S-Au complexes, rendering the proposed reaction thermodynamically feasible. In contrast, ejection of the formal Au-S complex with a DFT-derived energy cost of +1.94 eV is highly unfavourable. Unfortunately, it is not possible to clarify the elementary steps of the reaction mechanism, but a dissociative process where the C-S-Au-S-C linkages are entirely broken with the aid of Au adatoms appears feasible, and would be favoured at higher temperatures.

Accordingly, the additional sulfur species in XPS that occurred at higher binding energies after annealing at 250 °C arises from the ejected sulfur, and possibly traces back to adsorbed Au-S-Au complexes. The formation of sulfur molecules in subsequent surface reactions appears also possible, and would be consistent with a S 2p core level shift to higher binding energies. The coexistence of coordinative and covalent bonds as observed by STM (*cf.* Supporting Information) as well as the increasing amount of the additional sulfur species in XPS with progressive heating both consistently indicate a gradual conversion. Moreover, the close to 50:50 ratio of tentatively assigned ejected sulfur and thioether sulfur obtained after annealing at 300 °C suggests a nearly complete conversion. However, appearance of chemisorbed sulfur in XPS also marks the onset of decomposition. Even though the proposed reaction mechanism cannot be experimentally verified, additional surface sensitive vibrational spectroscopy as Electron Energy Loss Spectroscopy (EELS) or Infrared Reflection Absorption Spectroscopy (IRRAS) could contribute to independently confirm the thioether linkages or even identify reaction byproducts.

The third main question concerning emergence of STs is more intricate. As discussed above, the conversion of the thiolate S-Au-S linkages into covalent C-S-C thioether bonds proceeds gradually, *i.e.* in a sequential manner. Such a process initially leads to smaller covalent aggregates as dimers or trimers as basic units for subsequent structure formation. In order to understand whether these basic units are suitable precursors for the observed fractals, Monte Carlo (MC) simulations were performed. MC simulations are highly useful in this context as they could previously explain the formation of similar fractals from ditopic linkers.[17, 29] Cyclic trimers would be ideal precursors for the STs, because they already represent a complete structural subunit by themselves. Yet, DFT simulations of thioether linked dimers *versus* cyclic trimers result in almost similar energies per bond, hence exclude a pronounced energetic

preference for trimerization by cooperative effects. However, as shown in Figure 8, MC simulations based on thioether linked motif 4 dimers with an idealized C-S-C bond angle of 120° similarly result in ST (*cf.* Supporting Information for a video of the time evolution). Common structural features between MC simulations and STM experiments further support this hypothesis (*cf.* Supporting Information).
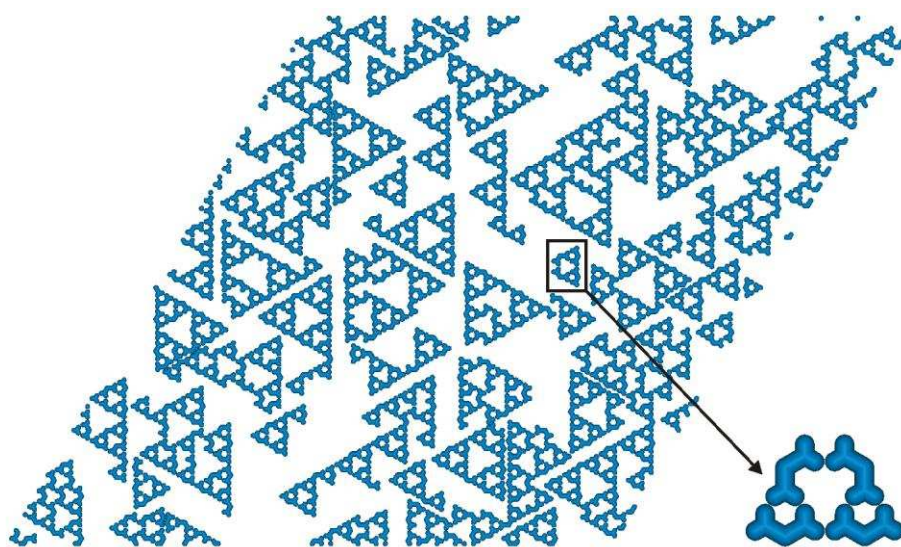
Figure 8. Representative result of a MC simulation based on rigid motif 4 dimers as basic building blocks. The sulfur atoms in the thioether linkages are not depicted for clarity. The close-up at the lower right highlights one possibility how four dimer building blocks can assemble into STs.

It is noteworthy that in these MC simulations the bonds are in principle reversible. However, the relatively low temperatures of the presented MC runs render detachment highly improbable. Interestingly, another series of MC simulations based on monomers yielded similar fractals, when the growing aggregates become immobile already at the dimer stage (*cf.* Supporting

Information), suggesting that combination of the threefold molecular symmetry with the 120°
bond angle already plays a decisive role for ST formation. Interestingly, the size of STs appears
to be limited to second generation both in experiments and MC simulations. The most likely
reason for this is the absence of classical ripening and coalescence mechanisms known from the
self-assembly of ordered monolayers as discussed in detail in previous work.[30] Accordingly, the
size limitation arises from kinetic effects.

In contrast to the STs, the dimers of oppositely oriented molecules observed after the final
annealing step at 300 °C are relatively trivial to explain. Their straight geometry already suggest
the absence of sulfur, and indeed the geometry perfectly matches with a covalent dimer based on
a C-C interlink (*cf.* Figure 5c and Supporting Information). These STM observations are in
accord with the appearance of chemisorbed sulfur in XPS. These high temperature annealing
experiments demonstrate that sulfur can be completely expelled from thioethers with subsequent
formation of C-C bonds. Besides these covalent C-C linked dimers, thioether linked motif 4
dimers as well as zero generation STs can still be identified in agreement with XPS. However,
not all structures can unambiguously be identified solely based on STM images and might also
exhibit chemically deviant linkages.

CONCLUSIONS

In summary, TMB on Au(111) is a particularly rich example for the formation of versatile
molecular nanostructures on surfaces, because it combines a range of important phenomena as
kinetic trapping, coordinative bonding to adatoms, hierarchical chirality, polymorphism,
dynamic reconfiguration, templated self-assembly, chemical changes of intermolecular bond
type, formation of regular fractals, and partial decomposition.

After room temperature deposition of TMB onto Au(111), deprotonation initiates the formation of intermolecular S-Au-S linkages with Au adatoms. The resulting aggregates are mostly disordered due to kinetic trapping, but can be reduced to only three basic intermolecular binding motifs. Mild annealing promotes formation of two types of regular 1D chains, both based on the room temperature binding motifs. Initially, it may appear surprising that a tritopic molecule as TMB does not form 2D but only 1D structures. However, the dominant motif 1 that is present in both types of chains is a twofold link. Accordingly, there is only one free mercaptophenyl group per molecule left, resulting in a motif 1 dimer with two sticky ends at *para* position – a prototypical secondary building block for linear polymers. The chain polymorphism again is related to the energetic equivalence of motifs 2 and 3 which are the single linkages interconnecting the dimers into chains. Interestingly, the chirality of binding motif 2 does not only extend along the chains, but is even preserved to the level of molecular braids – an example of hierarchical chirality.

The most interesting and surprising experimental observation is the conversion of Au-thiolate chains into regular fractals, the STs. These triangles are constituted of only one intermolecular binding motif 4 with similarly oriented molecules. A linear periodic continuation of motif 4 leads to type C chains that were only observed along step-edges – an example of templated self-assembly. Attempts of rationalizing the STs with S-Au-S thiolate linkages by geometric matching were not successful. The experimental bond lengths are markedly shorter and can only be explained by covalent thioether bonds. As a result, the structural transition from chains to triangles is driven by a chemical transition, where coordinative S-Au-S linkages are converted into covalent C-S-C bonds. The mechanism of this conversion is not entirely clear, but ejection of just the formal Au-S unit is energetically highly unfavorable. However, ejection of Au-S-Au

complexes formed with Au adatoms at higher surface temperatures is a chemically and thermodynamically plausible mechanism. Self-assembly of the fractals, on the other hand, is clearly reproduced by Monte Carlo simulations with covalent dimers or even just monomers as basic building blocks. In comparison, recent studies on ST self-assembly employed V-shaped tectons with *m*-terphenyl backbone. Here threefold halogen, hydrogen, or metal-coordination bonds gave rise to the triangular topology, whereas the twofold 120° connections between the triangle centers were realized by the *m*-terphenyl backbone. For TMB derived ST the situation is reverse: the threefold topology is encoded in the molecular structure, whereas the ~120° geometry of the thioether linkages provides the required connectivity.

In addition to the microscopic characterization, XPS provided information on the chemical environment of sulfur. Interestingly, the structurally most important chemical change from Au-thiolate to thioether is not monitored by XPS, because S 2p binding energies do not shift to a measurable extent. However, according to the proposed mechanism, sulfur is also ejected. Hence, an additional sulfur species that appeared in XPS at higher binding energies after annealing was assigned to this reaction byproduct. The chemical state of the ejected sulfur is not entirely clear, but a physisorbed species appears likely and would be in accord with XPS. Both STM and XPS consistently indicate a gradual transition. However, after a thermal treatment where XPS indicated complete conversion of thiolate into thioether, the onset of decomposition was observed both in STM and in XPS.

On Au(111) the emergence of STs was quite robust in the intermediate coverage range studied here. While lower coverages presumably just lead to step-edge decoration, studies at higher coverages approaching one monolayer might indeed be interesting. For hydrogen bonded STs Zhang *et al.* observed the coexistence of STs and periodic structures with increasing coverages.[15]

Accordingly, carrying out similar studies for the present system with its covalent intermolecular linkages could reveal further insights into bond reversibility of the thioether linkages. An important point that deserves future attention is the generality of the proposed surface chemistry, *i.e.* whether a similar conversion into thioether linkages also occurs for other flat adsorbing thiol functionalized molecules on Au(111) surfaces. In any case, an important lesson learnt from the present study is that even profound chemical changes are not necessarily detectable in high resolution XPS experiments. This underlines once more the importance of combined microscopic and spectroscopic studies for the field of on-surface synthesis.

MATERIALS AND METHODS

Experiments.

All sample preparations and experiments were performed under ultra-high vacuum conditions at a base pressure below 3×10^{-10} mbar. Epitaxial Au(111) films on mica (Georg Albert Physical Vapor Deposition, Silz, Germany) were used as substrates and prepared by cycles of Ne^+ (or Ar^+) ion-sputtering at 0.5 keV and annealing at ~750 K. The surface cleanliness was proven either by STM imaging or XPS prior to deposition. The synthesis of TMB was described previously,[11] and deposition was carried out by means of a home-built evaporator[31] at a crucible temperature of ~140 °C onto the surface held at room temperature, resulting in surface coverages of 0.35 ± 0.17 monolayers according to a statistical analysis of STM data. Full monolayer coverage refers to the densely packed $3\sqrt{3} \times 3\sqrt{3}R \pm 30°$ TMB superstructure observed on Cu(111),[11] corresponding to an area density of 0.656 molecules per nm^2. The coverages are slightly overestimated as STM imaging was preferentially carried out at surface areas with higher local coverage.

STM topographs were acquired with a home-built beetle type microscope driven by a SPM100 controller from RHK. Images were recorded in the constant current mode at room temperature and were leveled and mean value filtered. The bias voltage was applied from the sample to the tip.

XPS experiments were carried out at the BESSY II synchrotron (Helmholtz-Zentrum Berlin) at the HE-SGM beamline. The end station is a Prevac system, featuring separate preparation and analysis chambers. Sulfur 2p XP spectra were acquired with a photon energy of 330 eV at normal electron emission using a Scienta R3000 electron analyzer with a pass energy of 50 eV. Linear backgrounds were subtracted from all XP spectra. S 2p spin-orbit doublets were fitted with two Gaussians of equal width, applying a fixed energy separation of 1.2 eV and a fixed intensity ratio of 2:1 for the $p_{3/2}$:$p_{1/2}$ peak areas. Au $4f_{7/2}$ with a binding energy of 83.8 eV was used as internal energy reference. Molecular coverages in XPS experiments were comparable to those in STM experiments within ±20%. Owing to the absence of pronounced coverage dependencies, STM and XPS results correspond.

DFT simulations.

All dimer motifs, metal-organic, and covalent zero generation STs were simulated by DFT using the software Gaussian[32] with the B3LYP functional[33, 34] and LANL2DZ basis sets for all atoms.[35-37] Additional simulations with the PBE functional[38] resulted in similar geometries. Periodic type A and B chains as well as first generation metal-organic and covalent STs were simulated by DFT using the software CP2K[39, 40] with the PBE functional and DZVP basis sets for all atoms. CP2K calculations used periodic cells with a vertical dimension of 12 Å, while the dimensions in the lateral non-periodic directions were chosen so as to leave at least 7 Å vacuum between adjacent molecules or chains. Motif 2 dimers adsorbed on Au(111) structures were also

simulated using CP2K software and the PBE functional with the empirical dispersion correction (DFT-D2).[41] Owing to the large system size, the Au(111) surface was modelled using a single layer consisting of 10×14 unit cells with 140 Au atoms; the SZVP basis set was used for the Au surface atoms, and the DZVP basis set for the Au adatoms and all other atoms. Atomic positions in the single Au(111) layer were fixed, while the adsorbate was fully optimized.

MC simulations.

MC simulations used both monomers and dimers as basic building blocks. Monomers just consisted of four segments representing the phenyl rings. Dimers were modeled as rigid planar structures composed of nine interconnected segments, *i.e.* eight phenyl rings and one linking sulfur atom (*cf.* Supporting Information). The sulfur atoms of the thioether linkages between dimers were not explicitly considered, but implemented through the allowed bonding configurations, leaving an empty lattice site at the respective position of the sulfur atoms (*cf.* Supporting Information). In all simulations each of the segments was allowed to occupy one vertex (adsorption site) of a triangular lattice. This lattice defines adsorption sites and orientations of the dimers, but does not represent the actual Au(111) surface. Molecule-surface interactions were assumed to be equal for all lattice sites, *i.e.* the potential energy landscape of the surface was entirely flat. This simplification is justified by the relatively high formation temperature of the STs of ~250 °C where diffusion barriers are not playing a decisive role anymore. The simulations were performed on a 200×200 rhombic section of the lattice using the standard Monte Carlo method in canonical ensemble (CMC).[29, 42] Periodic boundary conditions were applied to minimize edge effects. Dimers were not allowed to overlap or occupy neighboring sites of the lattice. Bonding was only possible in configurations that feature a 120° bond angle (*cf.* Supporting Information). Each intermolecular bond resulted in a contribution to

the interaction energy of $\varepsilon = -1$; all other non-bonding intermolecular configurations resulted in a zero contribution to the interaction energy ($\varepsilon = 0$). According to the CMC formalism, the system size, number of adsorbed dimers N, and temperature T were fixed. The simulations started with a set of dimers at random positions with random orientations. The system was equilibrated by typically $10^6 \times N$ MC steps, where translation and rotation of dimers was attempted in each step. To this end, a dimer was selected at random and its potential energy E_0 evaluated in its current position with contributions from adjacent molecules equal to ε. Accordingly, only neighboring molecules in a bonding configuration contribute to E_0. Next, an attempt was made to move the selected dimer to a new position. The random translation of the dimer was accompanied by a random in-plane rotation by a multiple of 60° around its central segment. If all required lattice sites in the new position were unoccupied, the corresponding potential energy E_n was calculated using the same procedure as for E_0. If moving to the new position already resulted in an overlap with other dimers, the considered dimer was left in its original position. To accept the new position the conventional Metropolis criterion was used with the acceptance probability $p = min[1, \exp(-\Delta E/kT)]$, where $\Delta E = E_n - E_0$ and k is the Boltzmann constant. The calculated acceptance probability p was compared with a uniformly distributed random number $r\epsilon(0,1)$. If $r < p$ the new position was accepted, otherwise the move was discarded. The results reported herein were calculated for $N = 700$ and $T = 0.12$. The energies and temperatures are reduced values expressed in the units of ε and $|\varepsilon|/k$, respectively.

ASSOCIATED CONTENT

Supporting Information. Additional STM data (including a movie), additional DFT

simulations, MC details, MC simulations with monomer, and detailed comparison between MC

and STM; MC video. This material is available free of charge *via* the Internet at

http://pubs.acs.org.

AUTHOR INFORMATION

Corresponding Author

* Address correspondence to: markus@lackinger.org, www.2d-materials.com

Author Contributions

The manuscript was written through contributions of all authors. All authors have given approval

to the final version of the manuscript.

REFERENCES

1.   Nuzzo, R. G.; Allara, D. L. Adsorption of Bifunctional Organic Disulfides on Gold Surfaces. *J. Am. Chem. Soc.* **1983**, 105, 4481-4483.
2.   Whetten, R. L.; Khoury, J. T.; Alvarez, M. M.; Murthy, S.; Vezmar, I.; Wang, Z. L.; Stephens, P. W.; Cleveland, C. L.; Luedtke, W. D.; Landman, U. Nanocrystal Gold Molecules. *Adv. Mater.* **1996**, 8, 428-433.
3.   Templeton, A. C.; Wuelfing, W. P.; Murray, R. W. Monolayer-Protected Cluster Molecules. *Acc. Chem. Res.* **2000**, 33, 27-36.

4.   Reed, M. A.; Zhou, C.; Müller, C. J.; Burgin, T. P.; Tour, J. M. Conductance of a Molecular Junction. *Science* **1997**, 278, 252-254.

5.   Dorogi, M.; Gomez, J.; Osifchin, R.; Andres, R. P.; Reifenberger, R. Room-Temperature Coulomb Blockade from a Self-Assembled Molecular Nanostructure. *Phys. Rev. B* **1995**, 52, 9071-9077.

6.   Gittins, D. I.; Bethell, D.; Schiffrin, D. J.; Nichols, R. J. A Nanometre-Scale Electronic Switch Consisting of a Metal Cluster and Redox-Addressable Groups. *Nature* **2000**, 408, 67-69.

7.   Cui, X. D.; Primak, A.; Zarate, X.; Tomfohr, J.; Sankey, O. F.; Moore, A. L.; Moore, T. A.; Gust, D.; Harris, G.; Lindsay, S. M. Reproducible Measurement of Single-Molecule Conductivity. *Science* **2001**, 294, 571-574.

8.   Love, J. C.; Estroff, L. A.; Kriebel, J. K.; Nuzzo, R. G.; Whitesides, G. M. Self-Assembled Monolayers of Thiolates on Metals as a Form of Nanotechnology. *Chem. Rev.* **2005**, 105, 1103-1169.

9.   Vericat, C.; Vela, M. E.; Salvarezza, R. C. Self-Assembled Monolayers of Alkanethiols on Au(111): Surface Structures, Defects and Dynamics. *Phys. Chem. Chem. Phys.* **2005**, 7, 3258-3268.

10.   Maksymovych, P.; Sorescu, D. C.; Yates, J. T. Gold-Adatom-Mediated Bonding in Self-Assembled Short-Chain Alkanethiolate Species on the Au(111) Surface. *Phys. Rev. Lett.* **2006**, 97, 146103.

11.   Walch, H.; Dienstmaier, J.; Eder, G.; Gutzler, R.; Schlögl, S.; Sirtl, T.; Das, K.; Schmittel, M.; Lackinger, M. Extended Two-Dimensional Metal–Organic Frameworks Based on Thiolate–Copper Coordination Bonds. *J. Am. Chem. Soc.* **2011**, 133, 7909-7915.

12.   Marschall, M.; Reichert, J.; Weber-Bargioni, A.; Seufert, K.; Auwärter, W.; Klyatskaya, S.; Zoppellaro, G.; Ruben, M.; Barth, J. V. Random Two-Dimensional String Networks Based on Divergent Coordination Assembly. *Nat. Chem.* **2010**, 2, 131-137.

13.   Newkome, G. R.; Wang, P.; Moorefield, C. N.; Cho, T. J.; Mohapatra, P. P.; Li, S.; Hwang, S.-H.; Lukoyanova, O.; Echegoyen, L.; Palagallo, J. A.; Lancu, V.; Hla, S.-W. Nanoassembly of a Fractal Polymer: A Molecular "Sierpiński Hexagonal Gasket". *Science* **2006**, 312, 1782-1785.

14.   Shang, J.; Wang, Y.; Chen, M.; Dai, J.; Zhou, X.; Kuttner, J.; Hilt, G.; Shao, X.; Gottfried, J. M.; Wu, K. Assembling Molecular Sierpiński Triangle Fractals. *Nat. Chem.* **2015**, 7, 389-393.

15.   Zhang, X.; Li, N.; Gu, G. C.; Wang, H.; Nieckarz, D.; Szabelski, P.; He, Y.; Wang, Y.; Xie, C.; Shen, Z. Y.; Lu, J. T.; Tang, H.; Peng, L. M.; Hou, S. M.; Wu, K.; Wang, Y. F. Controlling Molecular Growth between Fractals and Crystals on Surfaces. *ACS Nano* **2015**, 9, 11909-11915.

16.   Zhang, X.; Li, N.; Liu, L. W.; Gu, G. C.; Li, C.; Tang, H.; Peng, L. M.; Hou, S. M.; Wang, Y. F. Robust Sierpiński Triangle Fractals on Symmetry-Mismatched Ag(100). *Chem. Commun.* **2016**, 52, 10578-10581.

17.   Li, N.; Zhang, X.; Gu, G. C.; Wang, H.; Nieckarz, D.; Szabelski, P.; He, Y.; Wang, Y.; Lue, J. T.; Tang, H.; Peng, L. M.; Hou, S. M.; Wu, K.; Wang, Y. F. Sierpiński-Triangle Fractal Crystals with the C_{3v} Point Group. *Chin. Chem. Lett.* **2015**, 26, 1198-1202.

18.   Sun, Q.; Cai, L. L.; Ma, H. H.; Yuan, C. X.; Xu, W. On-Surface Construction of a Metal-Organic Sierpiński Triangle. *Chem. Commun.* **2015**, 51, 14164-14166.

19.   Gu, G. C.; Li, N.; Liu, L. W.; Zhang, X.; Wu, Q. M.; Nieckarz, D.; Szabelski, P.; Peng, L. M.; Teo, B. K.; Hou, S. M.; Wang, Y. F. Growth of Covalently Bonded Sierpiński Triangles up to the Second Generation. *RSC Adv.* **2016**, 6, 66548-66552.

20.   Noh, J.; Ito, E.; Nakajima, K.; Kim, J.; Lee, H.; Hara, M. High-Resolution STM and XPS Studies of Thiophene Self-Assembled Monolayers on Au(111). *J. Phys. Chem. B* **2002**, 106, 7139-7141.

21.   Wang, H.; Chen, S.; Li, L.; Jiang, S. Improved Method for the Preparation of Carboxylic Acid and Amine Terminated Self-Assembled Monolayers of Alkanethiolates. *Langmuir* **2005**, 21, 2633-2636.

22.   Whelan, C. M.; Smyth, M. R.; Barnes, C. J. HREELS, XPS, and Electrochemical Study of Benzenethiol Adsorption on Au(111). *Langmuir* **1999**, 15, 116-126.

23.   Sirtl, T.; Jelic, J.; Meyer, J.; Das, K.; Heckl, W. M.; Moritz, W.; Rundgren, J.; Schmittel, M.; Reuter, K.; Lackinger, M. Adsorption Structure Determination of a Large Polyaromatic Trithiolate on Cu(111): Combination of Leed-I(V) and DFT-VdW. *Phys. Chem. Chem. Phys.* **2013**, 15, 11054-11060.

24.   Maksymovych, P.; Yates, J. T. Au Adatoms in Self-Assembly of Benzenethiol on the Au(111) Surface. *J. Am. Chem. Soc.* **2008**, 130, 7518-7519.

25.   Vance, A. L.; Willey, T. M.; Nelson, A. J.; van Buuren, T.; Bostedt, C.; Terminello, L. J.; Fox, G. A.; Engelhard, M.; Baer, D. XAS and XPS Characterization of Monolayers Derived from a Dithiol and Structurally Related Disulfide-Containing Polyamides. *Langmuir* **2002**, 18, 8123-8128.

26.   Ishida, T.; Choi, N.; Mizutani, W.; Tokumoto, H.; Kojima, I.; Azehara, H.; Hokari, H.; Akiba, U.; Fujihira, M. High-Resolution X-Ray Photoelectron Spectra of Organosulfur Monolayers on Au (111): S(2p) Spectral Dependence on Molecular Species. *Langmuir* **1999**, 15, 6799-6806.

27.   Yang, Y. W.; Fan, L. J. High-Resolution XPS Study of Decanethiol on Au(111): Single Sulfur-Gold Bonding Interaction. *Langmuir* **2002**, 18, 1157-1164.

28.   Angelova, P.; Solel, E.; Parvari, G.; Turchanin, A.; Botoshansky, M.; Gölzhäuser, A.; Keinan, E. Chemisorbed Monolayers of Corannulene Penta-Thioethers on Gold. *Langmuir* **2013**, 29, 2217-2223.

29.   Nieckarz, D.; Szabelski, P. Simulation of the Self-Assembly of Simple Molecular Bricks into Sierpiński Triangles. *Chem. Commun.* **2014**, 50, 6843-6845.

30.   Nieckarz, D.; Szabelski, P. Chiral and Fractal: From Simple Design Rules to Complex Supramolecular Constructs. *Chem. Commun.* **2016**, 52, 11642-11645.

31.   Gutzler, R.; Heckl, W. M.; Lackinger, M. Combination of a Knudsen Effusion Cell with a Quartz Crystal Microbalance: *In Situ* Measurement of Molecular Evaporation Rates with a Fully Functional Deposition Source. *Rev. Sci. Instrum.* **2010**, 81, 015108.

32.   Frisch, M. J.; Trucks, G. W.; Schlegel, H. B.; Scuseria, G. E.; Robb, M. A.; Cheeseman, J. R.; Scalmani, G.; Barone, V.; Mennucci, B.; Petersson, G. A.; Nakatsuji, H.; Caricato, M.; Li, X.; Hratchian, H. P.; Izmaylov, A. F.; Bloino, J.; Zheng, G.; Sonnenberg, J. L.; Hada, M.; Ehara, M.*; et al.* Gaussian 09, Revision D.01, Gaussian Inc., Wallingford Ct, 2013.

33.   Becke, A. D. Density-Functional Thermochemistry. III. The Role of Exact Exchange. *J. Chem. Phys.* **1993**, 98, 5648-5652.

34.   Lee, C.; Yang, W.; Parr, R. G. Development of the Colle-Salvetti Correlation-Energy Formula into a Functional of the Electron Density. *Phys. Rev. B* **1988**, 37, 785-789.

35.   Dunning Jr., T. H.; Hay, P. J. *Modern Theoretical Chemistry;* Ed. H. F. Schaefer III, Vol. 3, Plenum, New York, 1977, pp 1-28.

36.   Hay, P. J.; Wadt, W. R. *Ab Initio* Effective Core Potentials for Molecular Calculations. Potentials for the Transition Metal Atoms Sc to Hg. *J. Chem. Phys.* **1985**, 82, 270-283.

37.   Hay, P. J.; Wadt, W. R. *Ab Initio* Effective Core Potentials for Molecular Calculations. Potentials for K to Au Including the Outermost Core Orbitals. *J. Chem. Phys.* **1985**, 82, 299-310.

38.   Perdew, J. P.; Burke, K.; Ernzerhof, M. Generalized Gradient Approximation Made Simple. *Phys. Rev. Lett.* **1996**, 77, 3865-3868.

39.   VandeVondele, J.; Krack, M.; Mohamed, F.; Parrinello, M.; Chassaing, T.; Hutter, J. Quickstep: Fast and Accurate Density Functional Calculations Using a Mixed Gaussian and Plane Waves Approach. *Comput. Phys. Commun.* **2005**, 167, 103-128.

40.   Hutter, J.; Iannuzzi, M.; Schiffmann, F.; VandeVondele, J. CP2K: Atomistic Simulations of Condensed Matter Systems. *WIREs Comput. Mol. Sci.* **2014**, 4, 15-25.

41.   Grimme, S. Semiempirical GGA-Type Density Functional Constructed with a Long-Range Dispersion Correction. *J. Comput. Chem.* **2006**, 27, 1787-1799.

42.   Frenkel, D.; Smit, B. *Understanding Molecular Simulation: From Algorithms to Applications;* Academic Press, 2002, pp 1-638.

From Au-Thiolate Chains to Thioether Sierpiński Triangles: The Versatile Surface Chemistry of 1,3,5-Tris(4-Bercaptophenyl)Benzene on Au(111)

Atena Rastgoo-Lahrood, Natalia Martsinovich, Matthias Lischka, Johanna Eichhorn, Pawel Szabelski, Damian Nieckarz, Thomas Strunskus, Kalpataru Das, Michael Schmittel, Wolfgang M. Heckl, and Markus Lackinger